Journal of Sound and Vibration (1998) **214**(3), 513–529
Article No. sv981550

PARAMETRIC RESONANCE OF A ROTATING CYLINDRICAL SHELL SUBJECTED TO PERIODIC AXIAL LOADS

T. Y. NG AND K. Y. LAM

Department of Mechanical and Production Engineering, National University of Singapore, 10 Kent Ridge Crescent, 119260 Singapore

AND

J. N. REDDY

Department of Mechanical Engineering, Texas A and M University, College Station, Texas 77843-3123, U.S.A.

(*Received* 30 *June* 1997, *and in final form* 2 *February* 1998)

The parametric resonance of rotating cylindrical shells under periodic axial loading is investigated. The formulation is based on the dynamic version of Donnell's equation for thin rotating cylindrical shells. A modified assumed-mode method is used to reduce the partial differential equations of motion to a system of coupled second order differential equations with periodic coefficients of the Mathieu–Hill type. The instability regions are determined based on the principle of Bolotin's method. Of special interest here are the effects of the centrifugal and Coriolis forces on the instability regions which were examined in detail.

1. INTRODUCTION

Dynamic studies of rotating cylindrical shells have been of interest ever since Bryan [1], Di-Taranto and Lessen [2] and Srinivasan and Lauterbach [3] discovered the phenomenon of travelling modes and the effects of Coriolis forces. Free vibrations of rotating cylindrical rings and shells has been widely studied in many different forms. Mizoguchi [4] investigated the case in which a shell is treated as a beam and studied its critical speed. The effect of boundary conditions on the free vibration of prestressed rotating cylindrical shells has been studied by Penzes and Kraus [5]. The effects of constant axial pressures and torques on the natural frequencies of rotating prestressed cylinders were examined by Padovan [6], while studies on the effect of initial stresses were carried out by Armenakas and Herrmann [7, 8]. The use of different shell theories in the free vibration analysis of rotating composite cylindrical shells has been reported by Lam and Loy [9]. At the same time, great strides have also been made regarding the rotating ring problem by various authors [10–12].

To the knowledge of the authors, no publication is available in the open literature that reports the effect of rotation on the dynamic stability of rotating cylindrical shells. The articles mentioned above concentrated mainly on free vibration analysis. The present study was undertaken to report the effect of rotation on dynamic stability, as it would shed light on the effects of centrifugal and Coriolis forces in the prediction of the instability regions.

0022–460X/98/280513 + 17 $30.00/0

2. FORMULATION

The cylindrical shell under consideration (see Figure 1) is assumed to be a thin, uniform shell of length L, thickness h, radius R and rotating about the x-axis at constant angular velocity Ω. The elastic modulus is denoted by E, mass density by ρ and Poisson's ratio by v. The x-axis is taken along a generator, the circumferential arc length subtends an angle θ, and the z-axis is directed radially inwards. The non-dimensional periodic extensional axial load per unit length denoted by η_a. Donnell's thin shell theory is used to analyze the shell. The governing equations of motion of the cylindrical shell are

$$R^2 \frac{\partial^2 u}{\partial x^2} + \tfrac{1}{2}(1-v)\frac{\partial^2 u}{\partial \theta^2} + \frac{R}{2}(1+v)\frac{\partial^2 v}{\partial x\,\partial \theta} + vR\frac{\partial w}{\partial x} + \frac{\gamma}{\rho h}\tilde{N}_\theta\left(\frac{1}{R^2}\frac{\partial^2 u}{\partial \theta^2} - \frac{1}{R}\frac{\partial w}{\partial x}\right) = \gamma\frac{\partial^2 u}{\partial t^2}, \tag{1}$$

$$\frac{R}{2}(1+v)\frac{\partial^2 u}{\partial x\,\partial \theta} + \frac{R^2}{2}(1-v)\frac{\partial^2 v}{\partial x^2} + \frac{\partial^2 v}{\partial \theta^2} + \frac{\partial w}{\partial \theta} + \frac{\gamma}{\rho h}\tilde{N}_\theta\frac{1}{R}\frac{\partial^2 u}{\partial x\,\partial \theta} = \gamma\left(\frac{\partial^2 v}{\partial t^2} + 2\Omega\frac{\partial w}{\partial t} - \Omega^2 c\right), \tag{2}$$

$$-vR\frac{\partial u}{\partial x} - \frac{\partial v}{\partial \theta} - w - k\left(R^4\frac{\partial^4 w}{\partial x^4} + 2R^2\frac{\partial^4 w}{\partial x^2\,\partial \theta^2} + \frac{\partial^4 w}{\partial \theta^4}\right) + \frac{\gamma}{\rho h}\tilde{N}_\theta\left(\frac{1}{R^2}\frac{\partial^2 w}{\partial \theta^2} - \frac{1}{R^2}\frac{\partial v}{\partial \theta}\right)$$
$$+ R^2\frac{\partial}{\partial x}\left(\eta_a\frac{\partial w}{\partial x}\right) = \gamma\left(\frac{\partial^2 w}{\partial t^2} - 2\Omega\frac{\partial v}{\partial t} - \Omega^2 w\right), \tag{3}$$

where u, v and w are the displacements of a point on the reference surface of the shell, $\tilde{N}_\theta$ is the initial hoop tension due to the centrifugal force

$$\tilde{N}_\theta = \rho h \Omega^2 R^2 \tag{4}$$

and

$$\gamma = \rho R^2(1-v^2)/E, \qquad k = h^2/12R^2. \tag{5}$$

The nondimensional periodic extensional axial load is given by

$$\eta_a = \eta_0 + \eta_s \cos Pt, \tag{6}$$

where P is the frequency of excitation in radians per unit time and η_a, η_0 and η_s are non-dimensionalized by

$$\eta_a = N_a(1-v^2)/Eh, \qquad \eta_0 = N_0(1-v^2)/Eh, \qquad \eta_s = N_s(1-v^2)/Eh, \tag{7}$$

where N_a is the axial loading per unit length (Nm^{-1}) with N_0 being the constant component and N_s being the oscillatory component.

Assuming the shell to be simply supported, there exists a solution for the equations of motion in the form

$$u_{mn} = A_{mn}\cos\lambda_m x\cos(n\theta + \omega t), \qquad v_{mn} = B_{mn}\sin\lambda_m x\sin(n\theta + \omega t),$$
$$w_{mn} = C_{mn}\sin\lambda_m x\cos(n\theta + \omega t), \tag{8–10}$$

where n represents the number of circumferential waves, m the number of axial half-waves in the corresponding standing wave pattern and $\lambda_m = m\pi/L$. ω is the natural frequency of the rotating shell.

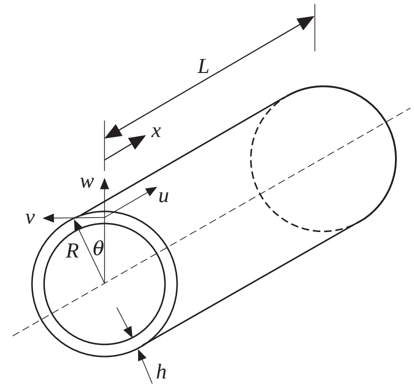

Figure 1. Co-ordinate system of the rotating circular cylindrical shell.

There exist six distinct natural frequencies for every combination of m and n. It has been concluded by Huang and Hsu [13] that in most engineering applications, the transverse modes dominate such that the contribution of in-plane modes; i.e., ω_{mnj}, $j = 3, 4, 5, 6$ can be neglected. Thus equations (8)–(10) can be expanded and simplified in terms of two generalized co-ordinates

$$u_{mnj} = \sum_{j=1}^{2} \sum_{m=1}^{\infty} \sum_{n=1}^{\infty} A_{mnj} \{ p_{mnj}(t) \cos n\theta - q_{mnj}(t) \sin n\theta \} \cos \lambda_m x, \tag{11}$$

TABLE 1

Unstable regions for the transverse modes of a simply-supported isotropic rotating cylindrical shell of $v = 0{\cdot}3$ and geometric properties $L/R = 2$ and $R/h = 100$ and subjected to extensional loading of $\eta_0 = 0{\cdot}1\eta_{cr}$

	Mode (1, 1)					
	Forward mode			Backward mode		
$\bar{\Omega}$	p_1	p_2	Θ $(\times 10^{-3})$	p_1	p_2	Θ $(\times 10^{-3})$
0	1·147165172	1·147165172	0·772328	–	–	–
$0{\cdot}1\bar{\varpi}_{0,(1,1)}$	1·135055631	1·135546954	0·788492	1·148134539	1·148452040	0·788492
$0{\cdot}2\bar{\varpi}_{0,(1,1)}$	1·097115252	1·101764719	0·812459	1·149670622	1·152898296	0·812459
	Mode (1, 2)					
0	0·658453850	0·658453850	1·654853	–	–	–
$0{\cdot}1\bar{\varpi}_{0,(1,2)}$	0·660645770	0·660734758	1·649010	0·664148968	0·664207985	1·649010
$0{\cdot}2\bar{\varpi}_{0,(1,2)}$	0·666789969	0·667580332	1·622727	0·680877888	0·681423345	1·622727
	Mode (1, 3)					
0	0·398573686	0·398573686	3·030464	–	–	–
$0{\cdot}1\bar{\varpi}_{0,(1,3)}$	0·409713576	0·409728301	2·945905	0·410713765	0·410724968	2·945905
$0{\cdot}2\bar{\varpi}_{0,(1,3)}$	0·441256764	0·441384513	2·727168	0·445268926	0·445366124	2·727168
	Mode (1, 4)					
0	0·276508010	0·276508010	4·577005	–	–	–
$0{\cdot}1\bar{\varpi}_{0,(1,4)}$	0·293580177	0·293583747	4·310424	0·293962023	0·293964978	4·310424
$0{\cdot}2\bar{\varpi}_{0,(1,4)}$	0·339573021	0·339603495	3·724128	0·341102775	0·341127545	3·724128

$$v_{mnj} = \sum_{j=1}^{2} \sum_{m=1}^{\infty} \sum_{n=1}^{\infty} B_{mnj} \{p_{mnj}(t) \sin n\theta + q_{mnj}(t) \cos n\theta\} \sin \lambda_m x, \tag{12}$$

$$w_{mnj} = \sum_{j=1}^{2} \sum_{m=1}^{\infty} \sum_{n=1}^{\infty} C_{mnj} \{p_{mnj}(t) \cos n\theta - q_{mnj}(t) \sin n\theta\} \sin \lambda_m x, \tag{13}$$

where $p_{mnj}(t)$ and $q_{mnj}(t)$ the two generalized co-ordinates.

Substituting equations (11)–(13) into equations (1)–(3) and multiplying equation (1) separately by $\alpha_{rsi} \cos \lambda_r x \cos s\theta$ and $\alpha_{rsi} \cos \lambda_r x \sin s\theta$, equation (2) separately by $\beta_{rsi} \sin \lambda_r x \sin s\theta$ and $\beta_{rsi} \sin \lambda_r x \cos s\theta$ and equation (3) separately by $\sin \lambda_r x \cos s\theta$ and $\sin \lambda_r x \sin s\theta$, where

$$\alpha_{mnj} = A_{mnj}/C_{mnj}, \qquad \beta_{mnj} = B_{mnj}/C_{mnj}, \tag{14}$$

and integrating over the surface and making use of the orthogonality condition, one obtains

$$\mathbf{M}^* \ddot{\mathbf{f}} + \mathbf{G}^* \dot{\mathbf{f}} + \{\mathbf{K}^* - \cos Pt \mathbf{Q}^*\} \mathbf{f} = 0, \tag{15}$$

TABLE 2

Unstable regions for the transverse modes of a simply-supported isotropic rotating cylindrical shell of $\nu = 0{\cdot}3$ *and geometric properties* $L/R = 2$ *and* $R/h = 100$ *and subjected to compressive loading of* $\eta_0 = -0{\cdot}1\eta_{cr}$

	Mode (1, 1)					
	Forward mode			Backward mode		
$\bar{\Omega}$	p_1	p_2	Θ $(\times 10^{-3})$	p_1	p_2	Θ $(\times 10^{-3})$
0	1·144069348	1·144069348	0·775349	–	–	–
$0{\cdot}1\bar{\omega}_{0,(1,1)}$	1·131958865	1·132453476	0·791627	1·145032457	1·145351874	0·791627
$0{\cdot}2\bar{\omega}_{0,(1,1)}$	1·094008455	1·098686908	0·815751	1·146544791	1·149790110	0·815751
	Mode (1, 2)					
0	0·651795592	0·651795592	1·672259	–	–	–
$0{\cdot}1\bar{\omega}_{0,(1,2)}$	0·654031013	0·654121038	1·666084	0·657533847	0·657593071	1·666084
$0{\cdot}2\bar{\omega}_{0,(1,2)}$	0·660304704	0·661095357	1·638880	0·674386364	0·674934110	1·638880
	Mode (1, 3)					
0	0·386237353	0·386237353	3·127144	–	–	–
$0{\cdot}1\bar{\omega}_{0,(1,3)}$	0·397739203	0·397753934	3·031888	0·398739131	0·398750396	3·031888
$0{\cdot}2\bar{\omega}_{0,(1,3)}$	0·430203220	0·430331023	2·760305	0·434213984	0·434311984	2·760305
	Mode (1, 4)					
0	0·257468320	0·257468320	4·912519	–	–	–
$0{\cdot}1\bar{\omega}_{0,(1,4)}$	0·275734659	0·275738229	4·587067	0·276116429	0·276119416	4·587067
$0{\cdot}2\bar{\omega}_{0,(1,4)}$	0·324295407	0·324325911	3·898189	0·325824780	0·325849834	3·898189

TABLE 3

Unstable regions for the transverse modes of a simply-supported isotropic rotating cylindrical shell of $\nu = 0{\cdot}3$ and geometric properties $L/R = 2$ and $R/h = 100$ and subjected to extensional loading of $\eta_0 = 0{\cdot}2\eta_{cr}$

$\bar{\Omega}$	Forward mode p_1	Forward mode p_2	Forward mode Θ ($\times 10^{-3}$)	Backward mode p_1	Backward mode p_2	Backward mode Θ ($\times 10^{-3}$)
	Mode (1, 1)					
0	1·148708534	1·148708534	1·541357	–	–	–
$0{\cdot}1\bar{\omega}_{0,(1,1)}$	1·136566352	1·137058133	1·573649	1·149683220	1·150001163	1·573649
$0{\cdot}2\bar{\omega}_{0,(1,1)}$	1·098524061	1·103179847	1·621501	1·151230985	1·154464835	1·621501
	Mode (1, 2)					
0	0·661757096	0·661757096	3·290644	–	–	–
$0{\cdot}1\bar{\omega}_{0,(1,2)}$	0·663948603	0·664039002	3·279140	0·667487860	0·667547702	3·279140
$0{\cdot}2\bar{\omega}_{0,(1,2)}$	0·670086295	0·670889278	3·227013	0·684319898	0·684873200	3·227013
	Mode (1, 3)					
0	0·404600426	0·404600426	5·959703	–	–	–
$0{\cdot}1\bar{\omega}_{0,(1,3)}$	0·415900308	0·415915727	5·794085	0·416931168	0·416942848	5·794085
$0{\cdot}2\bar{\omega}_{0,(1,3)}$	0·447893739	0·448027657	5·365205	0·452029291	0·452130772	5·365205
	Mode (1, 4)					
0	0·285551987	0·285551987	8·832163	–	–	–
$0{\cdot}1\bar{\omega}_{0,(1,4)}$	0·303175834	0·303179503	8·321157	0·303583126	0·303586370	8·321157
$0{\cdot}2\bar{\omega}_{0,(1,4)}$	0·350652264	0·350685936	7·195134	0·352284133	0·352311316	7·195134

where the matrices $\mathbf{M}^*$, $\mathbf{G}^*$, $\mathbf{K}^*$ and $\mathbf{Q}^*$ are given by

$$\mathbf{M}^* = \begin{bmatrix} \mathbf{M}_{IJ} & \mathbf{0} \\ \mathbf{0} & \mathbf{M}_{IJ} \end{bmatrix}, \qquad \mathbf{K}^* = \begin{bmatrix} \mathbf{K}_{IJ} & \mathbf{0} \\ \mathbf{0} & \mathbf{K}_{IJ} \end{bmatrix},$$

$$\mathbf{G}^* = \begin{bmatrix} \mathbf{0} & -\mathbf{G}_{IJ} \\ \mathbf{G}_{IJ} & \mathbf{0} \end{bmatrix}, \qquad \mathbf{Q}^* = \begin{bmatrix} \mathbf{Q}_{IJ} & \mathbf{0} \\ \mathbf{0} & \mathbf{Q}_{IJ} \end{bmatrix}, \tag{16, 17}$$

and $\ddot{\mathbf{f}}$, $\dot{\mathbf{f}}$ and $\mathbf{f}$ are column vectors defined as

$$\ddot{\mathbf{f}} = \begin{Bmatrix} \ddot{\mathbf{p}}_J \\ \ddot{\mathbf{q}}_J \end{Bmatrix}, \qquad \dot{\mathbf{f}} = \begin{Bmatrix} \dot{\mathbf{p}}_J \\ \dot{\mathbf{q}}_J \end{Bmatrix}, \qquad \mathbf{f} = \begin{Bmatrix} \mathbf{p}_J \\ \mathbf{q}_J \end{Bmatrix}. \tag{18}$$

The subscripts r, s, i, m, n, j, I and J used in equations (16)–(18) have the following ranges: $i, j = 1, 2$, $r, s, m, n = 1, 2, \ldots, N$ and $I, J = 1, 2, \ldots, 2N^2$.

The matrices $\mathbf{M}_{IJ}$, $\mathbf{K}_{IJ}$, $\mathbf{G}_{IJ}$ and $\mathbf{Q}_{IJ}$ are given as

$$\mathbf{M}_{IJ} = \begin{Bmatrix} \gamma(\pi L/2)(1 + \beta_I\beta_J + \alpha_I\alpha_J), & \text{if } I = J, \\ 0, & \text{if } I \neq J; \end{Bmatrix} \qquad \mathbf{K}_{IJ} = \begin{Bmatrix} (\pi L/2)K^*, & \text{if } I = J, \\ 0, & \text{if } I \neq J; \end{Bmatrix} \tag{19, 20}$$

TABLE 4

Unstable regions for the transverse modes of a simply-supported isotropic rotating cylindrical shell of $v = 0{\cdot}3$ and geometric properties $L/R = 2$ and $R/h = 100$ and subjected to compressive loading of $\eta_0 = -0{\cdot}2\eta_{cr}$

	Mode (1, 1)					
	Forward mode			Backward mode		
$\bar{\Omega}$	p_1	p_2	Θ ($\times 10^{-3}$)	p_1	p_2	Θ ($\times 10^{-3}$)
0	1·142516863	1·142516863	1·553489	–	–	–
$0{\cdot}1\bar{\omega}_{0,(1,1)}$	1·130372841	1·130871208	1·586185	1·143479049	1·143800824	1·586185
$0{\cdot}2\bar{\omega}_{0,(1,1)}$	1·092310337	1·097024311	1·634667	1·144979108	1·148248363	1·634667
	Mode (1, 2)					
0	0·648440048	0·648440048	3·360111	–	–	–
$0{\cdot}1\bar{\omega}_{0,(1,2)}$	0·650721518	0·650811928	3·347305	0·654257951	0·654318216	3·347305
$0{\cdot}2\bar{\omega}_{0,(1,2)}$	0·657118642	0·657922217	3·291470	0·671339596	0·671897545	3·291470
	Mode (1, 3)					
0	0·379918577	0·379918577	6·344903	–	–	–
$0{\cdot}1\bar{\omega}_{0,(1,3)}$	0·391964771	0·391980203	6·145655	0·391964771	0·391980203	6·145655
$0{\cdot}2\bar{\omega}_{0,(1,3)}$	0·425847546	0·425981581	5·640463	0·429980207	0·430083365	5·640463
	Mode (1, 4)					
0	0·247399372	0·247399372	10·16907	–	–	–
$0{\cdot}1\bar{\omega}_{0,(1,4)}$	0·267576262	0·267580198	9·409119	0·267983378	0·267986698	9·409119
$0{\cdot}2\bar{\omega}_{0,(1,4)}$	0·320429534	0·320463280	7·864383	0·322060584	0·322088397	7·864383

$$\mathbf{G}_{IJ} = \begin{cases} (\pi L/2)(2\gamma\Omega)(\beta_I + \beta_J), & \text{if } I = J, \\ 0, & \text{if } I \neq J; \end{cases} \qquad \mathbf{Q}_{IJ} = \begin{cases} -(\pi L/2)(R^2\lambda_m\lambda_r\eta_s), & \text{if } I = J, \\ 0, & \text{if } I \neq J; \end{cases} \tag{21, 22}$$

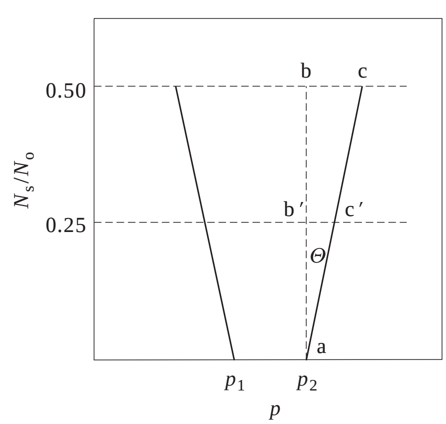

Figure 2. An unstable region in the N_s/N_0-p plane.

where

$$K^* = \alpha_I\alpha_J\left[(R\lambda_m)^2 + \frac{1-\nu}{2}n^2 + \frac{\tilde{N}_\theta}{\rho h}\frac{\gamma}{R^2}n^2\right] - \alpha_I\beta_J\left[\frac{1+\nu}{2}R\lambda_m n\right] - \alpha_I\left[\nu R\lambda_m - \frac{\tilde{N}_\theta}{\rho h}\frac{\gamma}{R}\lambda_m\right]$$

$$- \beta_I\alpha_J\left[\frac{1+\nu}{2}R\lambda_m n + \frac{\tilde{N}_\theta}{\rho h}\frac{\gamma}{R}\lambda_m n\right] + \beta_I\beta_J\left[\frac{1-\nu}{2}(R\lambda_m)^2 + n^2 - \gamma\Omega^2\right]$$

$$- \beta_I[-n] - \alpha_J[\nu R\lambda_m] - \beta_J\left[-n - \frac{\tilde{N}_\theta}{\rho h}\frac{\gamma}{R^2}n\right]$$

$$+ \left[k((R\lambda_m)^2 + n^2)^2 + 1 + \frac{\tilde{N}_\theta}{\rho h}\frac{\gamma}{R^2}n^2 - \gamma\Omega^2 + \eta_0(R\lambda_m)^2\right]. \quad (23)$$

3. STABILITY ANALYSIS

Equation (15) is in the form of a second order differential equation with periodic coefficients of the Mathieu–Hill type. The regions of unstable solutions are separated by periodic solutions having period T and $2T$ with $T = 2\pi/P$. The solutions with period $2T$ are of greater practical importance as the widths of these unstable regions are usually larger than those associated with solutions having period T. As a first approximation, the periodic solutions with period $2T$ can be sought in the form

$$\mathbf{f} = \mathbf{a}\sin(Pt/2) + \mathbf{b}\cos(Pt/2), \quad (24)$$

where $\mathbf{a}$ and $\mathbf{b}$ are arbitrary vectors.

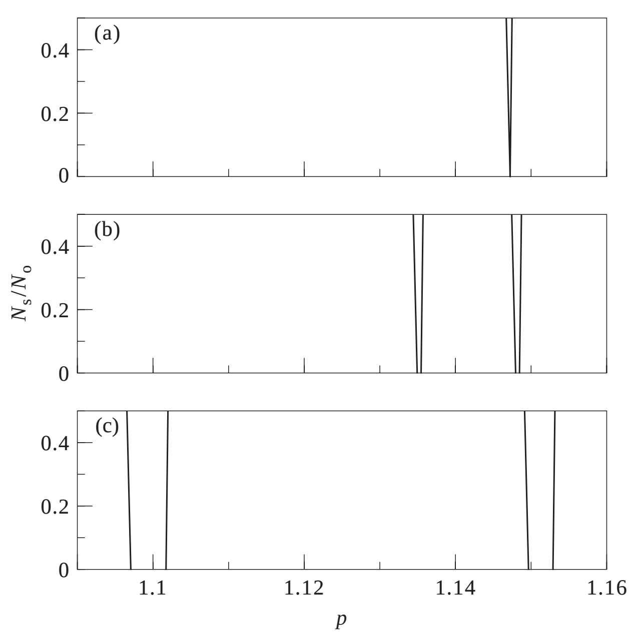

Figure 3. Unstable regions for the transverse mode of mode (1, 1) of a simply-supported isotropic rotating cylindrical shell of $\nu = 0{\cdot}3$ and geometric properties $L/R = 2$ and $R/h = 100$ and subjected to extensional loading of $\eta_0 = 0{\cdot}1\eta_{cr}$: (a) $\Omega = 0$; (b) $\Omega = 0{\cdot}1\bar{\omega}_{0(1,1)}$; (c) $\bar{\Omega} = 0{\cdot}2\bar{\omega}_{0(1,1)}$.

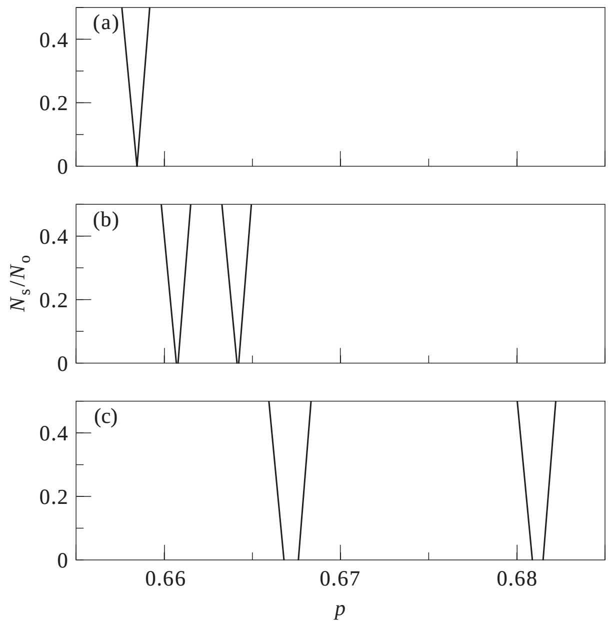

Figure 4. As Figure 3 but for mode (1, 2): (a) $\bar{\Omega} = 0$; (b) $\bar{\Omega} = 0{\cdot}1\bar{\omega}_{0(1,2)}$; (c) $\bar{\Omega} = 0{\cdot}2\bar{\omega}_{0(1,2)}$.

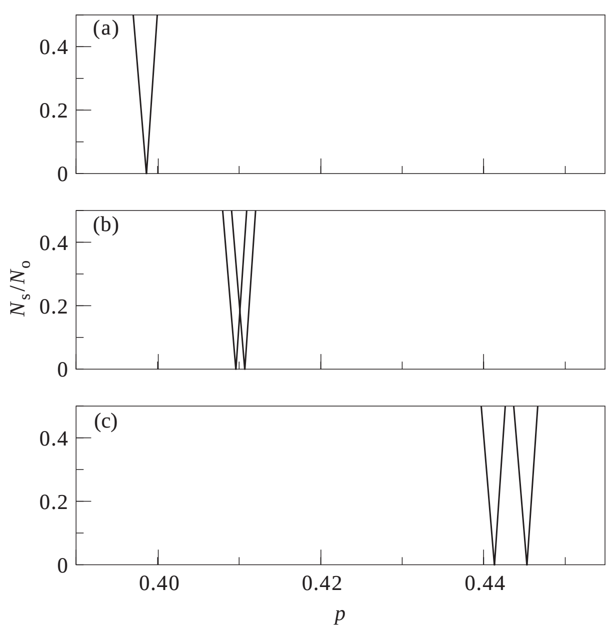

Figure 5. As Figure 3 but for mode (1, 3): (a) $\bar{\Omega} = 0$; (b) $\bar{\Omega} = 0{\cdot}1\bar{\omega}_{0(1,3)}$; (c) $\bar{\Omega} = 0{\cdot}2\bar{\omega}_{0(1,3)}$.

Substituting equation (26) into equation (15) and equating the coefficients of the $\sin(Pt/2)$ and $\cos(Pt/2)$ terms, a set of linear homogeneous algebraic equations in terms of $\mathbf{a}$ and $\mathbf{b}$ can be obtained. The conditions for non-trivial solutions are given by

$$\det\left[\begin{pmatrix} \mathbf{K}^* - \frac{1}{2}\mathbf{Q}^* - \frac{1}{4}P^2\mathbf{M}^* & \frac{1}{2}P\Omega\mathbf{G}^* \\ \frac{1}{2}P\Omega\mathbf{G}^* & \mathbf{K}^* + \frac{1}{2}\mathbf{Q}^* - \frac{1}{4}P^2\mathbf{M}^* \end{pmatrix}\right] = 0. \tag{25}$$

Equation (27) is the equation of boundary frequencies and can be used to calculate the boundaries of the instability regions.

4. NUMERICAL RESULTS AND DISCUSSION

The dynamic instability regions for the first order parametric resonances of a rotating cylindrical shell under combined static and periodic axial loads are presented in Tables 1 to 4 and Figures 1 to 18. The non-dimensional excitation frequency parameter p is defined as

$$p = RP\sqrt{\rho(1-v^2)/E}. \tag{26}$$

Each unstable region is bounded by two lines which may or may not originate from a common point from the p-axis. The two curves appear at first glance to be straight lines but are in fact two very slight "outward" curving plots. For the sake of tabular presentation, each unstable region is defined by its two originating points, p_1 and p_2, from the p-axis with $\eta_s = 0$. If the two curves originate from the same point, as is the case for non-rotating shell, then $p_1 = p_2$. The angle subtended, Θ, is also introduced. It is calculated based on the arctangent of the right-angled triangle, abc, as shown in Figure 2. This angle gives an accurate measurement of the slope of the boundary of the unstable region as calculations done with the smaller similar triangle, $ab'c'$ (see Figure 2), are within 0·1%.

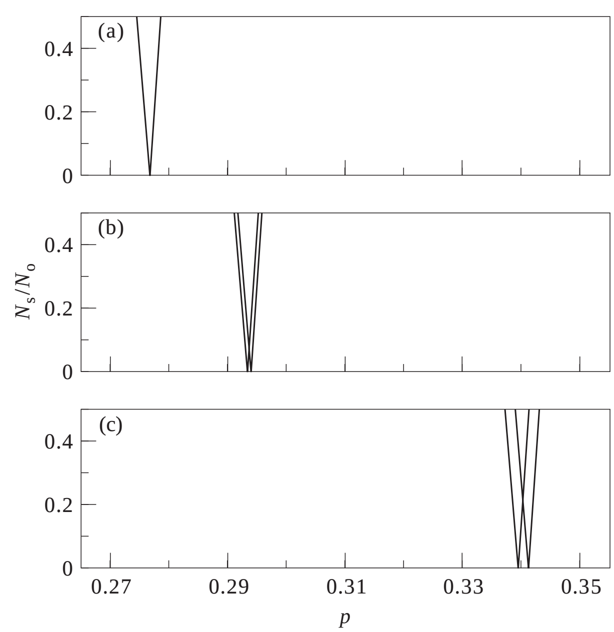

Figure 6. As Figure 3 but for mode (1, 4): (a) $\bar{\Omega} = 0$; (b) $\bar{\Omega} = 0{\cdot}1\bar{\omega}_{0(1,4)}$; (c) $\bar{\Omega} = 0{\cdot}2\bar{\omega}_{0(1,4)}$.

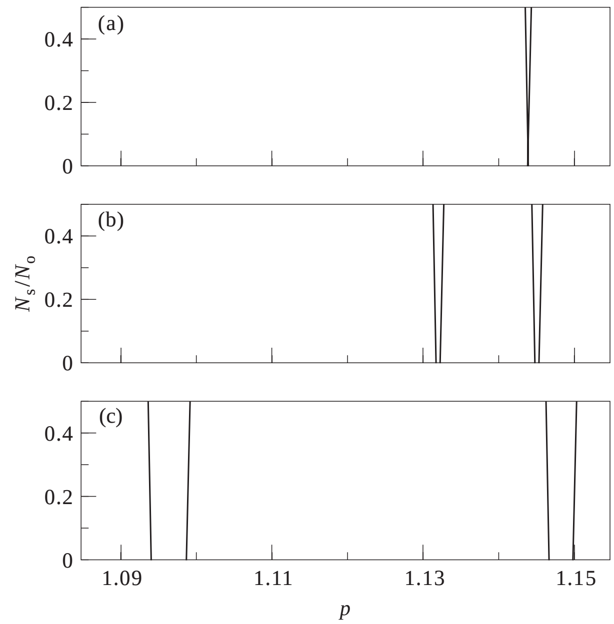

Figure 7. Unstable regions for the transverse mode (1, 1) of a simply-supported isotropic rotating cylindrical shell of $v = 0{\cdot}3$ and geometric properties $L/R = 2$ and $R/h = 100$ and subjected to compressive loading of $\eta_0 = -0{\cdot}1\eta_{cr}$: (a) $\bar{\Omega} = 0$; (b) $\bar{\Omega} = 0{\cdot}1\bar{\omega}_{0(1,1)}$; (c) $\bar{\Omega} = 0{\cdot}2\bar{\omega}_{0(1,1)}$.

The results presented in this study are for a simply-supported isotropic rotating cylindrical shell of $v = 0{\cdot}3$ and geometric properties $L/R = 2$ and $R/h = 100$. The modes of interest here are the transverse modes and the two higher axial and circumferential modes are neglected in the analysis. Results presented are for different rotational speeds

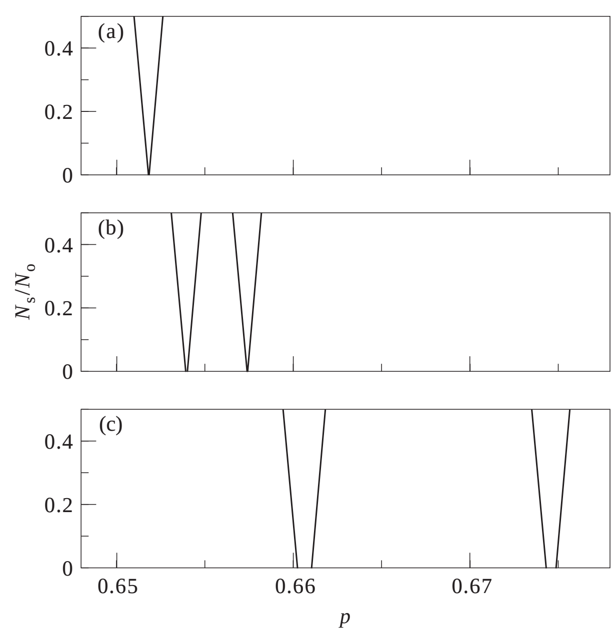

Figure 8. As Figure 7 but for mode (1, 2): (a) $\bar{\Omega} = 0$; (b) $\bar{\Omega} = 0{\cdot}1\bar{\omega}_{0(1,2)}$; (c) $\bar{\Omega} = 0{\cdot}2\bar{\omega}_{0(1,2)}$.

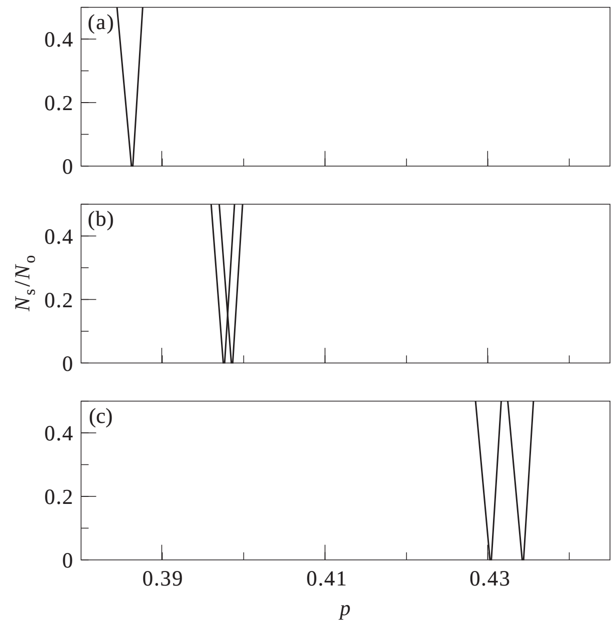

Figure 9. As Figure 7 but for mode (1, 3): (a) $\bar{\Omega} = 0$; (b) $\bar{\Omega} = 0{\cdot}1\bar{\omega}_{0(1,3)}$; (c) $\bar{\Omega} = 0{\cdot}2\bar{\omega}_{0(1,3)}$.

for the transverse modes of modes (1, 1), (1, 2), (1, 3) and (1, 4) respectively. The results presented here exclude those for circumferential wave number $n > 4$ due to the limitation of Donnell's equations to the higher circumferential modes for short to moderate length cylindrical shells.

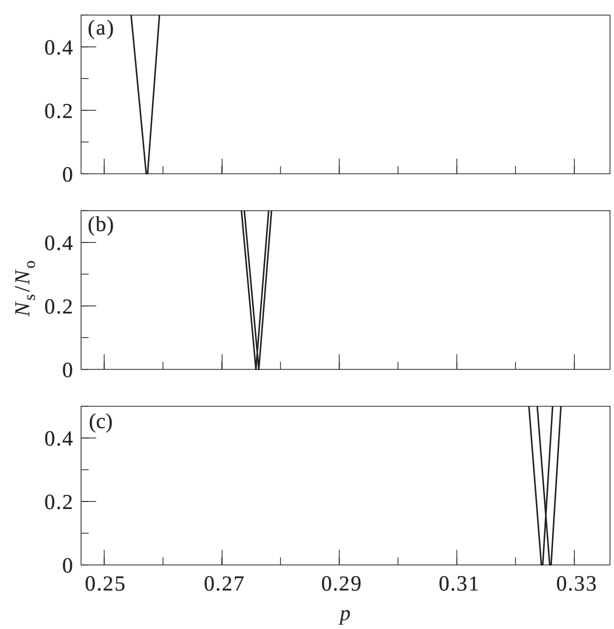

Figure 10. As Figure 7 but for mode (1, 4): (a) $\bar{\Omega} = 0$; (b) $\bar{\Omega} = 0{\cdot}1\bar{\omega}_{0(1,4)}$; (c) $\bar{\Omega} = 0{\cdot}2\bar{\omega}_{0(1,4)}$.

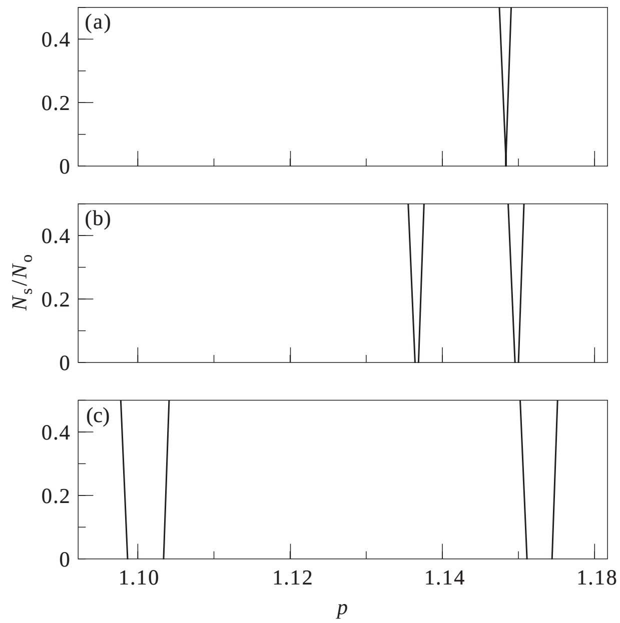

Figure 11. Unstable regions for the transverse mode of mode (1, 1) of a simply-supported isotropic rotating cylindrical shell of $v = 0{\cdot}3$ and geometric properties $L/R = 2$ and $R/h = 100$ and subjected to extensional loading of $\eta_0 = 0{\cdot}2\eta_{cr}$: (a) $\Omega = 0$; (b) $\Omega = 0{\cdot}1\bar{\omega}_{0(1,1)}$; (c) $\Omega = 0{\cdot}2\omega_{0(1,1)}$.

The values of η_0 are chosen to be in terms of η_{cr} which is the critical buckling load of a simly-supported circular cylindrical shell subjected to static compressive axial load and is given by

$$\eta_{cr} = N_{cr}([1 - v^2]/Eh), \tag{27}$$

where N_{cr} as given by Timoshenko and Gere [14] is

$$N_{cr} = Eh^2/[3(1 - v^2)]^{1/2}R \tag{28}$$

and if v is taken to be 0·3, then

$$\eta_{cr} = 0{\cdot}5507(h/R). \tag{29}$$

Table 1 gives the tabular representations for Figures 3–6, which contains results for tensile loading of $\eta_0 = 0{\cdot}1\eta_{cr}$. Corresponding results for compressive loading of $\eta_0 = -0{\cdot}1\eta_{cr}$ are given in Table 2 and Figures 7–10. The corresponding results for increased loading magnitudes are given in Table 3 and Figures 11–14 for tensile loading for $\eta_0 = 0{\cdot}2\eta_{cr}$ and in Table 4 and Figures 15–18 for compressive loading of $\eta_0 = -0{\cdot}2\eta_{cr}$. The tables are provided to give quantitative values to the unstable regions so that more accurate comparisons can be made between the different cases considered. Also they may be used as a source for comparison in future works by other authors for more complicated related problems.

The non-dimensional rotational speeds, $\bar{\Omega}$, used for each mode are in terms of the dimensionless natural frequencies of the non-rotating shell, $\bar{\omega}_0$, of that particular mode and under corresponding tensile loading. In the present case, due to the constraint of space, the two speeds considered are $\bar{\Omega} = 0{\cdot}1\bar{\omega}_0$, $0{\cdot}2\bar{\omega}_0$. These speeds were chosen as results obtained for the different transverse modes using these two speeds provided clear observations for the onset of the bifurcations of the instability regions which occur at lower

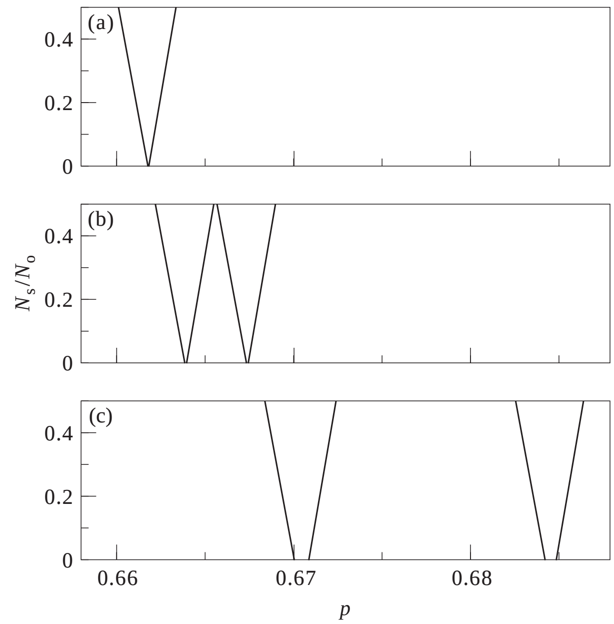

Figure 12. As Figure 11 but for mode (1, 2): (a) $\bar{\Omega} = 0$; (b) $\bar{\Omega} = 0{\cdot}1\bar{\omega}_{0(1,2)}$; (c) $\bar{\Omega} = 0{\cdot}2\bar{\omega}_{0(1,2)}$.

rotational speeds. Clear observations of the Coriolis effects which are larger for higher rotational speeds were also achieved using these two speeds.

It is noted from the results presented that the introduction of rotation generates two unstable regions for each transverse mode. This is expected as it is well known that the presence of rotation will cause the natural frequencies to bifurcate due to the Coriolis

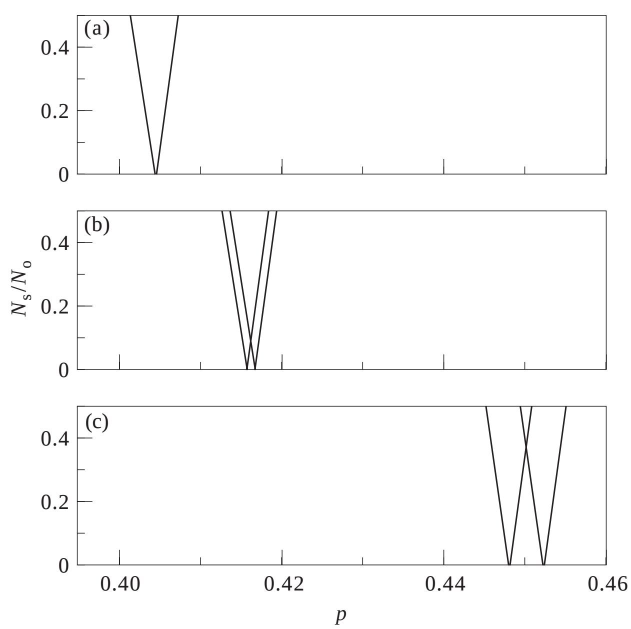

Figure 13. As Figure 11 but for mode (1, 3): (a) $\bar{\Omega} = 0$; (b) $\bar{\Omega} = 0{\cdot}1\bar{\omega}_{0(1,3)}$; (c) $\bar{\Omega} = 0{\cdot}2\bar{\omega}_{0(1,3)}$.

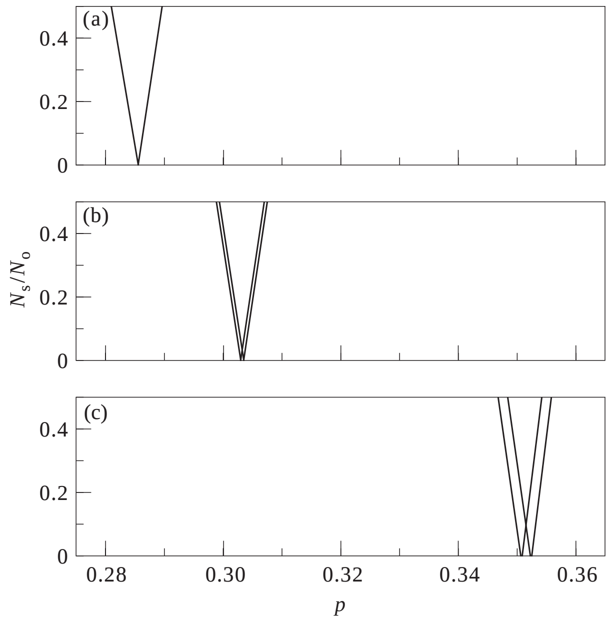

Figure 14. As Figure 11 but for mode (1, 4): (a) $\bar{\Omega} = 0$; (b) $\bar{\Omega} = 0{\cdot}1\bar{\omega}_{0(1,4)}$; (c) $\bar{\Omega} = 0{\cdot}2\bar{\omega}_{0(1,4)}$.

effects, one in the forward travelling mode and the other in the backward travelling mode. Thus the lower unstable region represents the forward mode and the higher unstable region represents the backward mode.

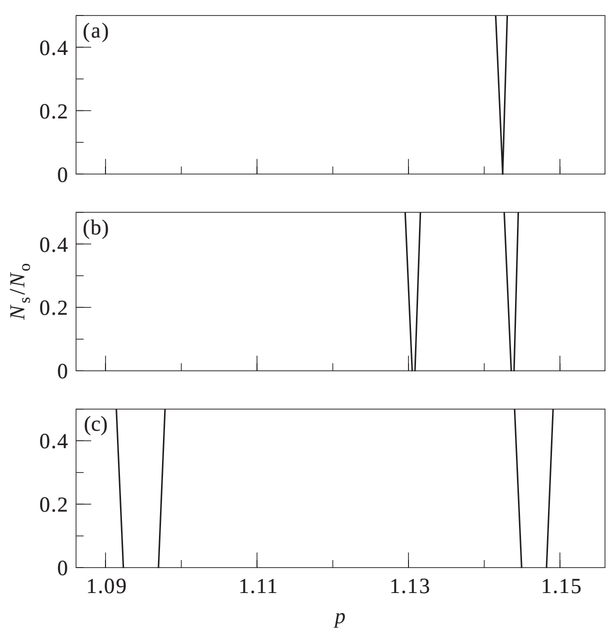

Figure 15. Unstable regions for the transverse mode of mode (1, 1) of a simply-supported isotropic rotating cylindrical shell of $v = 0{\cdot}3$ and geometric properties $L/R = 2$ and $R/h = 100$ and subjected to compressive loading of $\eta_0 = -0{\cdot}2\eta_{cr}$: (a) $\bar{\Omega} = 0$; (b) $\Omega = 0{\cdot}1\bar{\omega}_{0(1,1)}$; (c) $\bar{\Omega} = 0{\cdot}2\bar{\omega}_{0(1,1)}$.

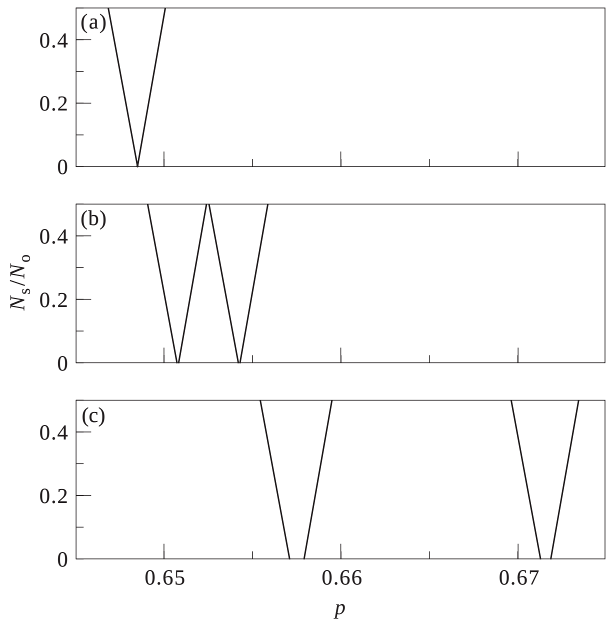

Figure 16. As Figure 15 but for mode (1, 2): (a) $\bar{\Omega} = 0$; (b) $\bar{\Omega} = 0{\cdot}1\bar{\omega}_{0(1,2)}$; (c) $\bar{\Omega} = 0{\cdot}2\bar{\omega}_{0(1,2)}$.

It is also observed that as the rotational speeds increase, the boundaries of the each unstable region shift away from each other and the region broadens. In some of the figures, this phenomena is not immediately apparent as the boundaries of the unstable regions for these cases have just begun to shift away from each other. However, the tabular results clearly show the presence of this phenomena. As the Coriolis terms are proportional to the rotational speed, it can be concluded that the Coriolis effects destabilizes the rotating shell causing the widths of the unstable regions to increase. It can also be concluded for the rotating shell configuration used in the present study, the lower modes of (1, 1) and (1, 2) are much more sensitive to the Coriolis effects than the higher modes of (1, 3) and (1, 4). It is also interesting to note from the results that for each respective mode, the shift of the boundaries away from each other is more pronounced in the forward wave than in the backward wave.

In some of the figures, it is observed that there is some overlapping between the unstable regions of the forward and backward waves especially at the initial bifurcation. The positive eigenvalues of the boundaries of the unstable regions corresponding to the backward waves are due to a positive rotation, $\Omega > 0$, while the negative eigenvalues of the boundaries of the unstable regions corresponding to the backward waves are due to a negative rotation, $\Omega < 0$. In the case of a stationary shell, these two eigenvalues are identical and the vibratory motion is a standing wave motion. However, if the shell begins to rotate, this standing wave motion is transformed and depending on the direction of rotation, backward or forward waves will emerge. Thus the overlapping should not be viewed as a superposing of two instabilities as they both cannot coexist at the same time for a particular rotating shell.

From the results, one may note that as the magnitude of the tensile loading is increased, the unstable regions shift to the right having higher points of origins. The converse is true when the magnitude of the compressive loading is increased. This can be expected in line with the argument that the natural frequencies of a shell increases as it is axially stretched

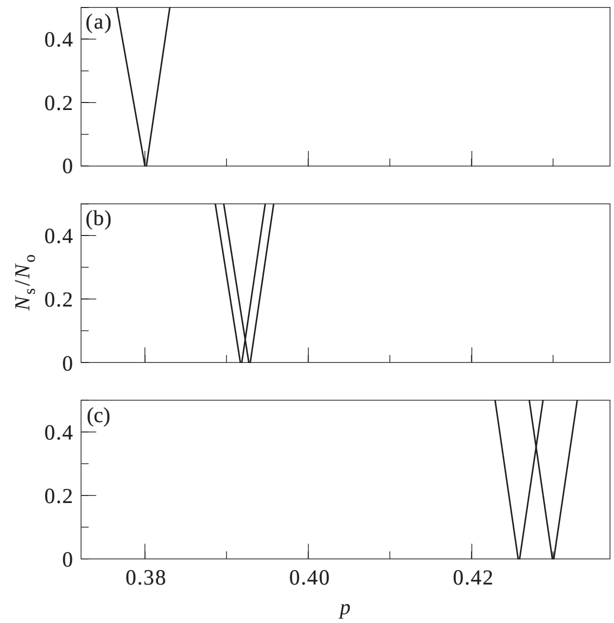

Figure 17. As Figure 15 but for mode (1, 3): (a) $\bar{\Omega} = 0$; (b) $\bar{\Omega} = 0{\cdot}1\bar{\omega}_{0(1,3)}$; (c) $\bar{\Omega} = 0{\cdot}2\bar{\omega}_{0(1,3)}$.

and decreases as it is compressed. The size of the unstable regions in this study is thus dependent upon two variables, firstly the $p_2 - p_1$ difference and secondly the subtended angle Θ. From the results, it is observed that as the magnitude of the axial loading is increased for both tensile and compressive cases, the sizes of the unstable regions also increase. It is also worthy to note that for tensile and compressive loadings of the same

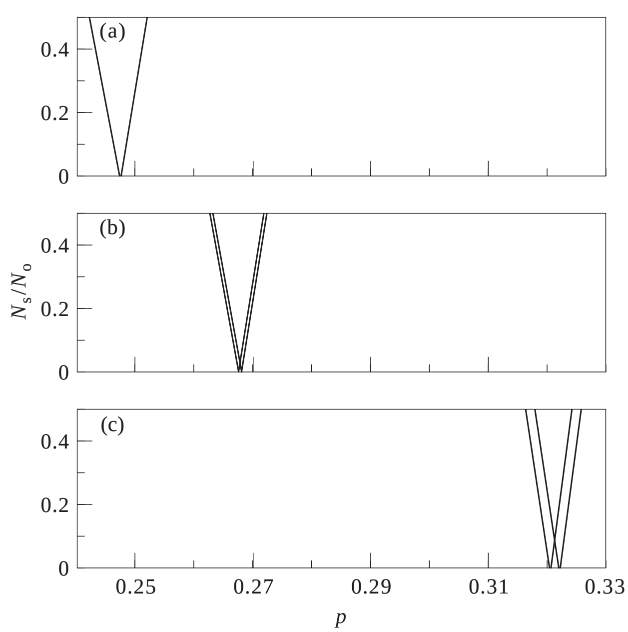

Figure 18. As Figure 15 but for mode (1, 4): (a) $\bar{\Omega} = 0$; (b) $\bar{\Omega} = 0{\cdot}1\bar{\omega}_{0(1,4)}$; (c) $\bar{\Omega} = 0{\cdot}2\bar{\omega}_{0(1,4)}$.

magnitude, the sizes of the unstable regions associated with the compressive loading is generally larger. Another interesting observation is that for any particular mode, the subtended angle Θ is the same for both its forward and backward wave.

5. CONCLUSIONS

The dynamic stability of simply-supported, isotropic rotating cylindrical shells under combined static and periodic axial forces was investigated. The Coriolis effects caused the generation of two unstable regions for each transverse mode. The Coriolis effects also caused the boundaries of the unstable regions to shift away from each other thus causing the sizes of the unstable regions to increase. The sizes of the unstables were also found to be generally larger for compressive loadings than for tensile loadings.

Extensions of the present study to cylindrical shells accounting for transverse shear deformation and to laminated composite cylindrical shells (see Reddy [15, 16]) with or without shear deformation awaits attention.

REFERENCES

1. G. H. Bryan 1890 *Proceedings of the Cambridge Philosophical Society* **7**, 101–111. On the beats in the vibration of revolving cylinder or bell.
2. R. A. DiTaranto and M. Lessen 1964 *ASME Journal of Applied Mechanics* **31**, 700–701. Coriolis acceleration effect on the vibration of a thin-walled circular cylinder.
3. A. V. Srinivasan and G. F. Lauterbach 1971 *ASME Journal of Engineering for Industry* **93**, 1229–1232. Traveling waves in rotating cylindrical shells.
4. K. Mizoguchi 1964 *Bulletin of the Japanese Society of Mechanical Engineers* **7**, 310–317. Vibration of a rotating cylindrical shell.
5. L. E. Penzes and H. Kraus 1972 *AIAA Journal* **10**, 1309–1313. Free vibration of prestressed cylindrical shells having arbitrary homogeneous boundary conditions.
6. J. Padovan 1973 *Journal of Sound and Vibration* **31**, 469–482. Natural frequencies of rotating prestressed cylinders.
7. A. E. Armenakas and G. Herrmann 1963 *AIAA Journal* **1**, 100–106. Vibrations of infinitely long cylindrical shells under initial stress.
8. G. Herrmann and A. E. Armenakas 1962 *Proceedings of the Fourth U.S. National Congress of Applied Mechanics*, 203–213. Dynamic behavior of cylindrical shells under initial stress.
9. K. Y. Lam and C. T. Loy 1995 *Journal of Sound and Vibration* **186**, 23–35. Analysis of rotating laminated cylindrical shells using different shell theories.
10. D. C. Johnson 1952 *Aircraft Engineering* **24**, 234–236. Free vibrations of a rotating elastic body.
11. C. W. Bert and T. L. C. Chen 1978 *Journal of Sound and Vibration* **61**, 517–530. On vibration of a thick flexible ring rotating at high speed.
12. M. Endo, K. Hatamura, M. Sakata and O. Taniguchi 1984 *Journal of Sound and Vibration* **92**, 261–272. Flxural vibration of a thin rotating ring.
13. S. C. Huang and B. S. Hsu 1990 *Journal of Sound and Vibration* **136**, 215–228. Resonant phenomena of a rotating cylindrical shell subjected to a harmonic moving load.
14. S. P. Timoshenko and J. M. Gere 1961 *Theory of Elastic Stability*. New York: McGraw-Hill.
15. J. N. Reddy 1994 *Energy and Variational Methods in Applied Mechanics*. New York: John Wiley.
16. J. N. Reddy 1997 *Mechanics of Laminated Composite Plates: Theory and Analysis*. Boca Raton, Florida: CRC Press.